Determining In-plane Diffusivity in Gas Diffusion Layers for Proton Exchange Membrane Fuel Cells

Schlatter, A.H.

Award date:
2025

Determining In-plane Diffusivity in Gas Diffusion Layers for Proton Exchange Membrane Fuel Cells

---

A.H. Schlatter - Master thesis

Examination committee:
Dr. ir. Antoni Forner Cuenca
Dr. ir. Kay Buist
Dr. Adrian Mularczyk
Ir. Rens Horst

Eindhoven, January 23, 2025

Abstract

An experimental study on the In-plane diffusivity of Gas Diffusion Layers (GDLs) for use in Proton Exchange Membrane Fuel Cells (PEMFCs) is presented. The transport characteristics of GDLs are of importance in optimizing the design of PEMFC. Diffusion of oxygen on the cathode side can be limiting in cell operation and is therefore a property of interest. A device is designed for measuring using direct transient oxygen measurements. A MATLAB model is developed and verified to analyze the data from this measuring setup. The working of this device could not be made to reliably reproduce literature values for bulk diffusion even through extensive troubleshooting. For this reason only qualitative experiments were done to compare the diffusivity of different GDLs and the impact of compression on diffusivity.

Contents

List of Figures

List of Tables

1 Introduction

The electrification of mobility and logistics is desirable for two reasons: The energy efficiency of electrical motors is far higher than that of internal combustion engines and, the emission of harmful exhaust gases can be reduced or eliminated entirely.

Electrical motors can have energy efficiencies of up to 96%[1] while internal combustion engines can have efficiencies of up to 54%[2]. Additionally, when electric vehicles are employed the emission of exhaust gases can be centralised at the power plants used to generate the electricity, where the waste stream can more easily be cleaned properly, or in the case of using renewable electricity no fossil fuel and thus no exhaust gases are needed.

The most prevalent technology for storing energy in electric vehicles is battery storage. Unfortunately, for some applications in mobility batteries are too heavy to be practically employed. In particular long haul trucking and aviation suffer from weight limitations[3]. For these applications using hydrogen fuel cells could be an interesting alternative as hydrogen is very energy dense per weight compared to gasoline or Li-ion batteries[3][4].

Out of the available fuel cell technologies, Proton Exchange Membrane Fuel Cells (PEMFCs) are the most mature technology for applications in mobility[5]. These cells use a proton exchange membrane that can transport the protons that are split from hydrogen on the anode side to the cathode side where they combine with oxygen ions to form water. The electrons generated at the anode side are used to exert the electrical work generated in the cell. Figure 1 shows a schematic representation of a PEMFC.

This image also shows the many transport phenomena occurring in the Gas Diffusion Layer (GDL) of the PEMFC. The GDL is a thin porous conductive layer used to facilitate the transport of electrons and reactants towards the catalyst and the transport of water and heat away from the catalyst. On the cathode side where water is formed by the fuel cell reaction transport occurs in three phases. Conduction of heat and electrons in the solid carbon of the GDL, gas convection and diffusion in the pores of the GDL, and the condensation, evaporation and capillary motion of water inside of the pores of the GDL. A good understanding of these transport processes and the influence they have on one another is an important factor in designing more effective fuel cells.

Since the most likely source of oxygen for mobility applications is the ambient air, oxygen diffusion towards the catalyst layer can in some case limit the performance of PEMFCs[7].

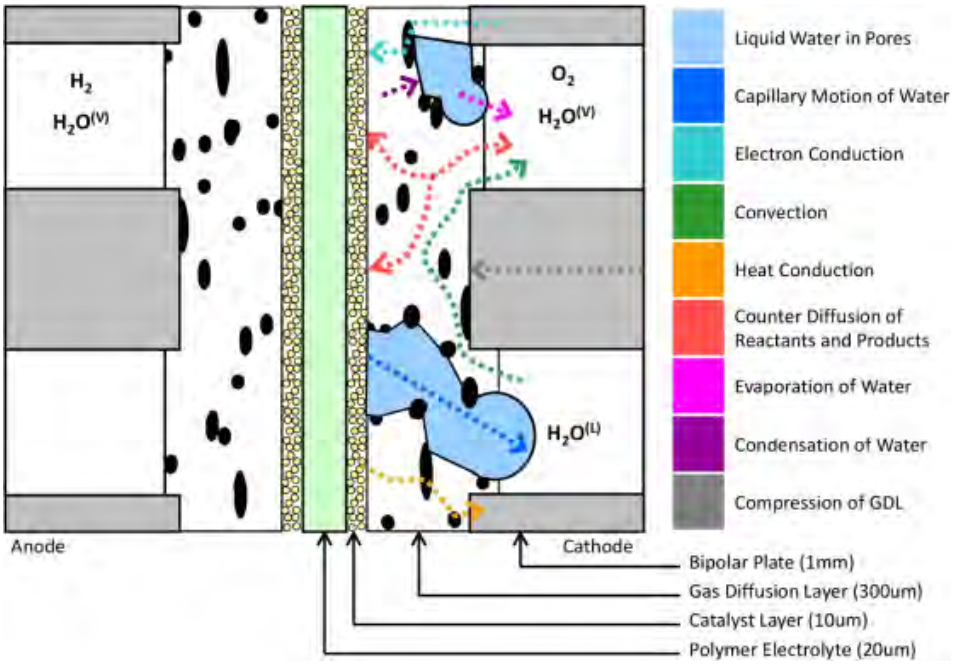

Figure 1: A schematic representation of a PEMFC[6]

As such understanding effective diffusion inside of these thin porous GDLs of importance for the optimization of PEMFCs. Another property of these GDL materials is their anisotropy. Several of the materials properties are different when viewing them in the plane of the material compared to viewing them through the plane of the material. Such at the electrical conductivity, the gas permeability and the effective diffusivity.

The thinness and conductivity of the cell components prevent many of the standard experimental methods for determining diffusivity in porous media from working. The conductivity of the materials makes it impossible to perform brine conductivity measurements. Where the limitation of the conductivity of the brine is analogous to the diffusion limitations. The thinness of the layers makes it difficult to control the initial and boundary conditions the diffusion models rely on to yield correct results. This makes standard devices such as Loschmidt or Wicke-Kallenbach(WK) cells very difficult to use reliably. Advances in sensor technology have made fast enough oxygen sensing possible that even for the fast diffusion processes in GDLs the time resolution is high enough to make sufficiently accurate concentration measurements to determine the diffusion coefficient in GDL materials.

2 Theory

A background is given on diffusion theory in bulk and porous media. The Gas Diffusion Layer and its impact on the performance of PEMFC performance is discussed. Finally the working principle of fluorescence based oxygen sensors is introduced.

2.1 Diffusion Theory

Free diffusion is caused by the random motion of molecules. One of the defining characteristics of diffusion is the tendency towards even concentration distributions across the domain of interest. Free diffusion is described by Fick's laws of which the first describes the mass flux as a function of the concentration gradient

$$\vec{J} = -D\nabla C \tag{1}$$

Where $\vec{J}$ is the mass flux of the species, C the concentration of the species and D the diffusion coefficient which is a proportionality constant dependent on the species that is diffusing and the medium its is diffusing in. Fick's second law can be derived from the first law by combining the first law with a mass conservation equation in absence of source terms

$$\frac{\partial C}{\partial t} + \nabla \cdot \vec{J} = 0 \tag{2}$$

Which yields the following equation assuming the diffusion coefficient is independent of concentration.

$$\frac{\partial C}{\partial t} = D\nabla^2 C \tag{3}$$

2.1.1 Binary gas diffusion

Diffusion of two gases in one another depends on the temperature and the pressure of the gas and, the two gases involved and the interactions between these molecules. The binary diffusion coefficient can be approximated well by Chapman-Enskog kinetic theory[8]. Which takes these three phenomena into account using the following equation

$$D_{AB} = \frac{3}{16}\sqrt{\frac{2\pi kT(m_A + m_B)}{m_A m_B}}\left(\frac{kT}{\pi\sigma_{AB}^2\Omega_D p}\right) \tag{4}$$

With k the Boltzmann constant, T the temperature of the gas. m_A and m_B the masses of gas A and B respectively, σ_{AB} is the mean of the collision radii of the involved gases, Ω_D is the collision integral of diffusion and, p is the pressure of the gas. The collision integral is a slowly varying function dependent on the temperature of the gas and the Lennard-Jones interaction parameter ϵ_{AB} which is dependent on the gases. This equation generally gives good predictions for the binary diffusion coefficient at low pressures with errors of 6-10% depending on whether the data for σ_{AB} and ϵ_{AB} were determined by viscosity or boiling point data[8].

2.2 Diffusion in porous media

Diffusion in fluids inside porous of media is restricted when compared to free fluids. This restriction is usually characterized with an effective diffusion coefficients or a diffusibility when D is independent of concentration. The diffusibility is the effective diffusivity normalized with the free diffusivity.

Diffusion in porous media occurs in the bulk regime when the sizes of the pores are significantly larger than the mean free path of the species in the fluids. In this situation the majority of interactions are molecule-molecule interactions while with smaller pores the impact of molecule-wall interactions becomes more influential. The free path in air is 70 nm, while in GDLs the pore sizes usually range from $10 - 100$ μm[9]. In the bulk regime the diffusion is only restricted by geometry which lengthens the diffusion paths and decreases the availability of these paths[10]. Several correlations exists to approximate effective diffusion coefficients for the bulk regime. These correlations are based on the porosity and tortuosity of the material. The porosity or the void fraction is the volumetric fraction of the material that can be filled with fluids.

$$\epsilon = \frac{V_{void}}{V_{sample}} \tag{5}$$

The tortuosity is a measure of the twistingness of a pathway. It is usually defined as

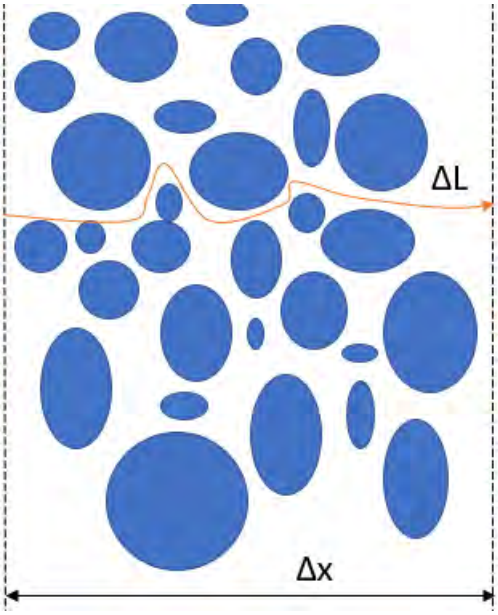

Figure 2: Illustration of tortuosity. Δx is the shortest path in an open medium and ΔL is the length of the path that the diffusion occurs in

$$\tau = \frac{\Delta L}{\Delta x} \tag{6}$$

Where ΔL is the length of the path the species takes while Δx is the shortest path in an open medium as shown in Figure 2. The most frequently used correlation relating the effective diffusion coefficient with the porosity and tortuosity of the sample is

$$D_{eff} = \frac{\epsilon}{\tau} D \tag{7}$$

2.3 Gas Diffusion Layers

In Proton Exchange Membrane Fuel Cells (PEMFCs) three phases are required to transport the reactants, the products and the charges to and away from the catalyst area where the reaction takes place. A solid phase for the transport of electrons and heat, a gas phase for the transport of hydrogen, oxygen, and water vapor and a liquid phase for the transport of the produced water out of the cell. In order to facilitate this transport Gas Diffusion Layers (GDLs) are employed. These porous materials are often based on polyacrylonitrile

fibers which are woven or stacked on top of each other and consequently carbonized at high temperatures[11]. This results in sheets with thicknesses in the range of $100 - 500\ \mu m$[9]. The carbon fibers are conductive and as such facilitate the transport of electrons while the voids in the material are used to transport the gases and water. Since diffusion of oxygen towards the catalyst layer can be a limiting factor[7], knowing the diffusion characteristics of these GDLs can lead to better design choices in designing PEMFCs.

2.3.1 Anisotropy of GDLs

In GDL materials it has been observed that due to the fibrous nature of GDLs the diffusion of gases inside the plane of the material is faster than diffusion through the plane of the material. Since diffusion in porous media in the bulk regime is inhibited by only the amount of available pathways, i.e. the porosity of the material, and the twistingness of these pathways, i.e. the tortuosity of the material. And since porosity is a quantity based on the volume of the material it cannot be different in either direction. Thus a difference in tortuosity must explain the difference between in-plane and through-plane diffusivity. Therefore, it would not be prudent to use any correlation for the effective diffusion coefficient that incorporates some relation where the tortuosity depends on the porosity of the material. This difference in tortuosity derives from the alignment of the fibers. As seen in Figure 3 the fibers lie stacked on top of on another in the through-plane direction. A diffusion pathway in the plane is much more likely to coincide with the direction of a fiber and while this pathway is running alongside the fiber it is not or negligibly tortuous. However, in the through-plane direction the diffusion pathways almost never align with the direction of a carbon fiber and as such these pathways are far more twisting than the in-plane paths.

2.4 Diffusion Impact on Cell Performance

Although currently the improvement of Oxygen Reduction Reaction is a major research topic within PEMFC research since the reduction or removal of platinum group metals as catalysts is desired. The diffusion of oxygen towards the electrode can also be limiting, especially considering water formation at this side of the cell further inhibits gas transport[7]. Furthermore since the reactants in this cell are neutral, migration cannot be used to enhance mass transfer. In electrochemical systems where diffusion is limiting the limiting current density can be expressed as

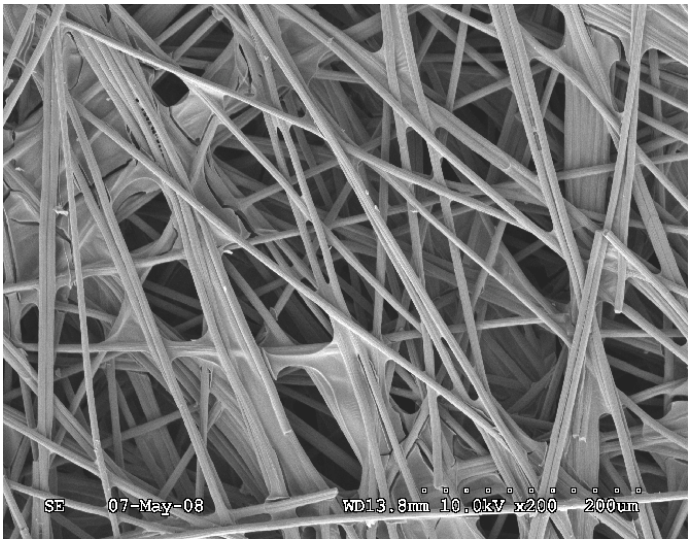

Figure 3: Top view of a Toray GDL[12]

$$j_{lim} = \frac{nFC_{bulk}D_{eff,O_2}}{\delta} \tag{8}$$

Where n represents the amount of electrons transferred, F the Faraday constant, C_{bulk} the bulk concentration of oxygen, D_{eff,O_2} the effective diffusion coefficient of oxygen and δ the thickness of the diffusion layer. The relation between the effective diffusion coefficient and the limiting current density is linear. However, it is important to note that during operation the effective diffusion coefficient can change due to the formation of liquid water at the cathode. In this diffusion limited case, increasing the effective diffusivity of the GDL will improve the performance of the cell. Additionally, increasing the diffusion performance reduces the likelihood of operating in a diffusion limited regime.

2.4.1 Influence of flow field, compression and GDL treatment on diffusion

In order to distribute gases into the fuel cell bipolar plates with structured channels for gas flow called flow fields are used. The two most commonly used flow fields are the parallel and interdigitated flow fields shown in Figure 4. In the parallel flow field the gas flows along the interface of the GDL while in an interdigitated flow field the gas is forced convectively through the GDL. A cross-sectional view of flow in these two flow field configurations is shown in Figure 5.

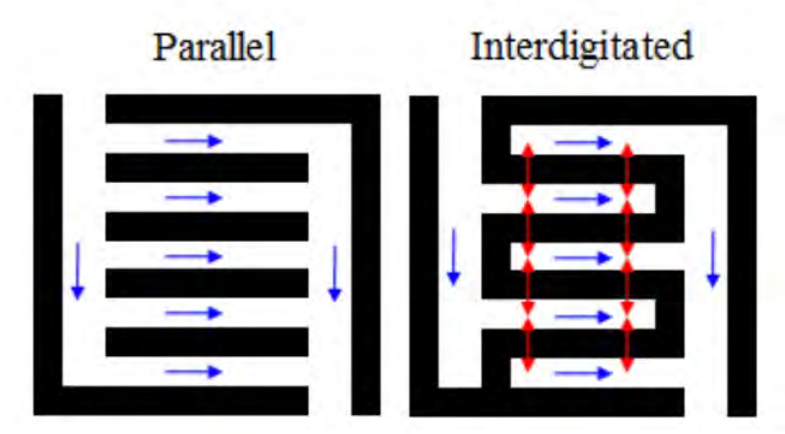

Figure 4: Different flow field geometries, blue arrows show main flow and red arrows show cross flow[13]

Especially in the case of a parallel flow field both in- and through-plane diffusion play a role. With interdigitated flow fields the convective flows increase the oxygen concentrations in the regions where the bipolar plate is in contact with the GDL. This increased mass transfer of interdigitated flow fields does come at the cost of higher pressure drop over the system. Another important factor in actual fuel cell operation is the compression required to make cells leak tight and to reduce the contact resistance between the current collectors and the GDL. However, compressing a GDL reduces the void space in the material and as such also reduces the available pathways for diffusion. The porosity of a material is given as

$$\epsilon = \frac{\epsilon_0 - C}{1 - C} \tag{9}$$

Where ϵ is the compressed porosity of the material, ϵ_0 the uncompressed porosity of the material, and C is the degree of compression expressed as $C = \frac{d}{d_0}$. With d and d_0 the compressed and uncompressed thicknesses respectively of the material. Finally GDLs for PEMFCs tend to be treated with PTFE or other polymers to make them more hydrophobic in order to better facilitate water transport away from the catalyst. This also has the side effect of blocking diffusion pathways and as such reduces the effective diffusivity of the GDL

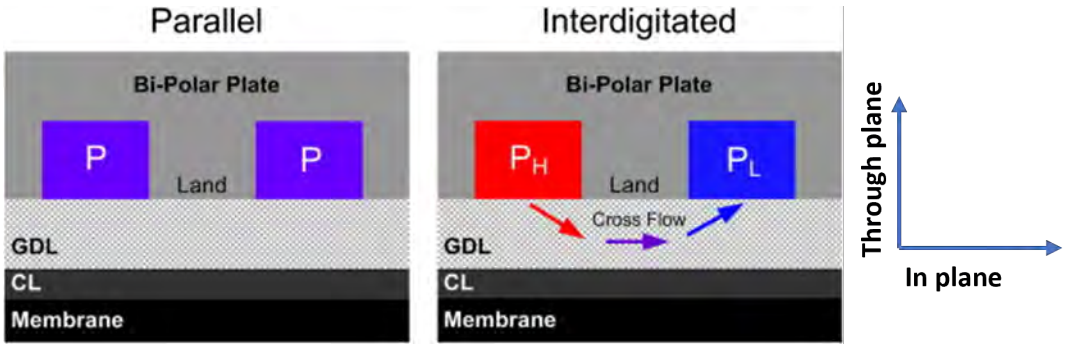

Figure 5: Side view of convective transport in a parallel and interdigitated flow field[14]

2.5 Fluorescence Quenching

Novel oxygen sensing technologies use the quenching properties of oxygen on certain fluorophores. This quenching provides an alternative pathway for the decay of the excited state without emitting light. The Stern-Volmer relationship describes the quenching process

$$\frac{I_0}{I} = 1 + k_q \tau_0 C_{O_2} \tag{10}$$

Where I and I_0 are the fluorescence intensity and the unquenched intensity respectively. k_q is the quenching rate coefficient, τ_0 is the lifetime of the excited species without a quencher present and C_{O_2} is the oxygen concentration. These sensors use a sinusoidal pulse of light in order to excite a fluorescent dye at the tip of a glass fiber. The returning signal is shifted in phase from the excited signal because of the time it takes for the excited state to fall back. The degree of this phase shift is dependent on the decay time of the excited state

$$\Delta\phi = arctan(\omega\tau) \tag{11}$$

Where $\Delta\phi$ is the phase shift, ω is the frequency of the pulse and τ is the lifetime of the excited state[15]. Since the quenching in these sensors are based on oxygen colliding with the fluorophore the excited states with longer lifetimes have a higher chance of colliding with the oxygen in the gas. Which has the result that a higher oxygen concentrations only the excited states with shorter lifetimes decay my emission while at low oxygen concentrations also the longer lifetime emission paths are available. This leads to an inverse relationship

between the phase shift and oxygen concentration

3 Method Selection

A proper method for measuring diffusivity in GDLs would need to accurately measure diffusion coefficients in short times while having the option of investigating effects that occur in PEMFCs which futher impact diffusion. Effects as compression of the GDL and the humidity of the gases inside of the GDL. Finally, the method proposed should be as cheap as possible. Four potential methods are investigated: Modified Loschmidt or Wicke-Kallenbach cells, transient oxygen diffusion experiments, and Electrochemical Impedance Spectroscopy (EIS).

3.1 Modified Loschmidt Cell

A regular Loschmidt cell consists of two compartments filled with different gases with a barrier separating the two compartments. To determine the binary diffusion coefficient of a gas mixture the barrier is opened for a certain time after which it is closed again and the contents of each compartment can be analyzed. This cell can be adapted for measuring a porous sample by including a porous sample near one side of the barrier. Translating the diffusion process into terms of mass transfer resistance [16]. Which is defined for a section i as

$$R_i = \frac{L_i}{D_i A_C} \tag{12}$$

With L_i the length of the section, D_i the diffusion coefficient in the section and A_C the cross sectional area where transport takes place. Figure 6 shows a schematic of the mass transfer network used in the experiments by Chan et al. [16]. The total mass transfer resistance of this network would be an addition of the individual resistances as they are all in series

$$R_{total} = R_{bulk,1} + R_{GDL} + R_{bulk,2} \tag{13}$$

Which gives when expanded

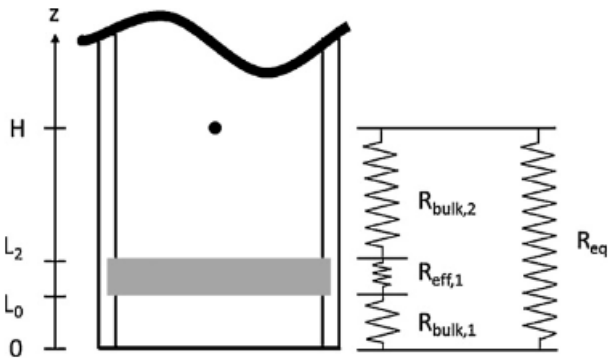

Figure 6: Schematic representation of a mass transfer resistance network, 0 represents the barrier between chambers, L_0 and L_2 the lower and upper part of the GDL sample and H is the location of the oxygen sensor [16]

$$\frac{H}{D_{total}A_C} = \frac{L_0}{D_{bulk}A_C} + \frac{L_2 - L_0}{D_{eff}A_C} + \frac{H - L_2}{D_{bulk}A_C} \tag{14}$$

The effective diffusion coefficient can be isolated from this expression

$$D_{eff} = \frac{L_2 - L_0}{\frac{H}{D_total} - \frac{H+L_0-L_2}{D_{bulk}}} \tag{15}$$

The effective diffusion coefficient of the complete system D_{total} can be determined experimentally and the bulk diffusion coefficient can be found in literature. However, determining D_{total} requires that the concentration of one of the gasses is measured transiently as the mixing that will still occur after the barrier is closed will muddy the contribution of the sample.

3.2 Wicke-Kallenbach cell

The Wicke-Kallenbach(WK) cell is an apparatus designed for measuring transport in porous media. It consists of two streams of different gases running parallel alongside opposing sides of a porous sample[17]. The composition of the output streams is monitored continuously. This method has been used for determining diffusivity in GDLs by Yoshimune et al[18] & Pant et al[19].

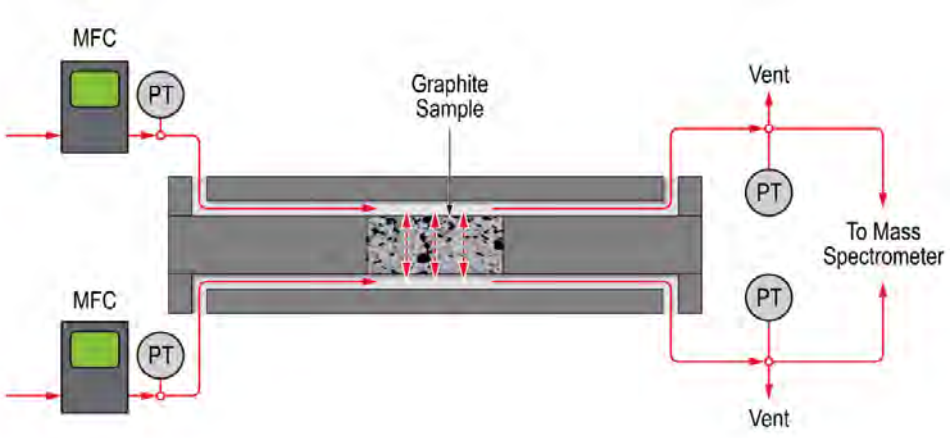

Figure 7: Schematic of a Wicke-Kallenbach cell[20]

Determining the diffusion coefficient from a WK cell is done by comparing the observed molecular flux through the sample extracted through measuring the composition of the inlet and outlet gases and the diffusion flux from Fick's law. Under the assumption that the diffusion coefficient is independent of concentration the effective diffusivity is given as [17]

$$D_{eff} = \frac{L}{A_C}(F_j y_i^L + F_i y_j^U) \tag{16}$$

Where L is the length of the sample, A_C is the cross sectional area available for transport, F_i is the molar flow rate of component i and y_i^L and y_j^U are the molar fractions of component A in the lower channel and component B in the upper channel respectively.

3.3 Transient Oxygen Measurement

Developments in oxygen sensing technology make it possible to take measurements fast enough ($\Delta t \approx 0.1\ s$) so that it becomes possible to measure gas diffusion transiently with sufficiently small time steps for determining the diffusion characteristics in thin transport media. These novel sensors use fluorescence quenching to measure the oxygen concentration. By measuring transient diffusion directly the effective diffusion coefficent can be directly calculated by fitting Fick's 2nd law to the concentration data. This has been done by Kim& Gostick [21] and Rashapov et al. [6]

3.4 Electrochemical Impedance Spectroscopy

A known analogous process to diffusion in porous media in the bulk regime is conductivity of electrolytes in porous media. This process encounters the same limitations of path length and blockage as diffusion does. Generally AC measurements at high frequencies ($f \approx 10kHz$) can be done in order to determine the conductivity of an electrolyte. Since these measurements are done at high frequencies kinetic effects are not expected to have a large influence[22]. However the presence of a GDL in the electrolyte influences the conductivity measurements due to the conductivity of the material leading to double layer formation between the electrolyte and the GDL. Kramer et al. [22] have used EIS to determine diffusion coefficients in GDL materials. The electrochemical system can be represented by a resistor and a fractal surface model element[23]. EIS could be used to investigate the range of impedances these double layers can have and through this analysis the contribution of the material and the electrolyte can be deconvoluted.

3.5 Final selection

The modified Loschmidt cell is promising for determining through plane diffusivity as it is very easy to eliminate potential contributions of convection to the mass transfer. For in plane diffusion the device would need to be very thin. However, this should not be a major problem. The aspect of GDL compression would be more difficult to investigate as the transport direction needs to remain open in order to properly assess D_{eff}. A strong disadvantage is the requirement for using a mass transfer resistance network model as it would be very hard to deconvolute anomalies occurring in the bulk diffusion from anomalies within the GDL.

The advantage of Wicke-Kallenbach cells is that they can give a value for diffusion in a steady state measurement. However, this relies on the size of convective flows by the porous sample when pressure fluctuations between the two gas streams occur. For thicker porous samples this is no issue as the contribution of convective flows is small compared to the contribution of diffusion in the material. This makes this setup viable for doing in plane diffusivity measurements as the width of the sample can chosen freely and this makes it possible to sufficiently dampen the influence convection. However, when investigating through plane diffusivity in these thin transport materials the convective contribution becomes so large that it impacts the measurement significantly or the convective flow completely pen-

etrates the sample at very low pressure differences. Furthermore, the roughness of the sample surface would also create eddies which would induce flow into the sample[24]. Very fine pressure control would be needed in order to properly prevent convection from influencing the results. Compression would likely be easy to implement in this system as would the humidification of the gas streams. The final great drawback is the cost of the cell as the analysis of the gases and tight pressure control is costly.

A main advantage of using transient oxygen measurements is that it can be used to very closely imitate the operating conditions of an electrochemical cell while still allowing enough design freedom to properly isolate the in plane and through plane diffusivity. However, in designing an apparatus the boundary and initial conditions need to be tightly controlled as also in these devices convection is a major concern for the validity of the results. Furthermore, the compression of the GDL can be taken into account more when constructing this device making for easy application. Additionally, since the diffusion processes in GDLs tend to be fast these direct experiments will also be fast. Finally the cost of a device like this is reasonable since it can be manufactured in house at the university.

Advantages of EIS are the quick experiment times and the availability of equipment at the university. The main disadvantage of this method is its sensitivity, EIS is very sensitive to outside influences and small differences inside of the system. Another disadvantage is that these measurement require the GDL to be filled with electrolyte. This is further from the gas phase processes that we would like to investigate. Additionally some of the GDLs we would like to investigate have some degree of hydrophobic treatment which would require the use of non-aqueous electrolytes[25] which further complicates this method.

When weighing the advantages and disadvantages of these different methods the decision was made to work with transient oxygen measurements. The main reason for this that the diffusion process occurring using this method is very close to the gas diffusion processes occurring in PEMFC GDLs. Additionally the low experiment times and costs are also attractive properties of this method.

4 Device Design

The main requirements for this design is to ensure that the boundary and initial conditions of the diffusion equation are properly attained in the physical system so that it is possible

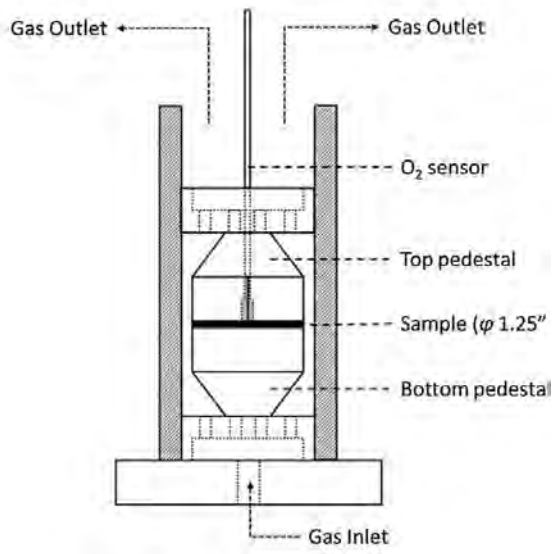

(a) Device design by Kim and Gostick

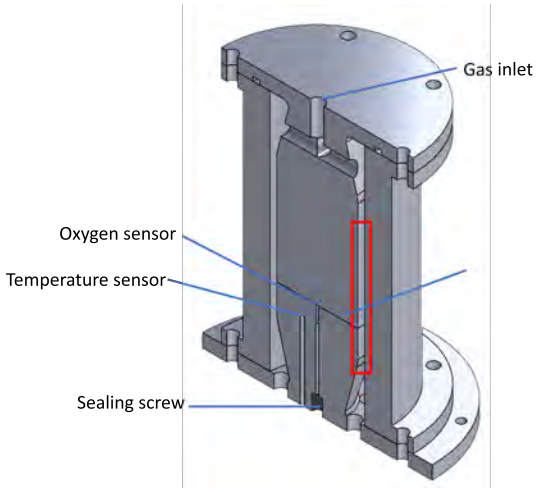

(b) Final design of the in-plane device. The red box denotes the area of the flow simulation in Figure 10a

Figure 8: Designs of Kim and Gostick and the in-plane device presented in this work

to extract a diffusion coefficient using a computational model.

4.1 In-plane

The design for the device measuring in-plane diffusion is based on the design by Kim and Gostick[21] as seen in Figure 8a. They implemented a cylindrical design which eliminates the requirement for sealing on two of the edges of the sample. The final design for the device used in this study can be seen in Figure 8b. The device consists of an outer cylinder with a top and a bottom lid. The top lid contains the gas connection for the nitrogen and compressed air lines. The bottom lid contains holes for the oxygen and temperature sensors. Also the bottom lid has a wider flange with holes for possible attachment points. These lids also have the two halves of the sample pedestal attached. The pedestal is 30 mm in diameter and the distance between the pedestal and the wall is 2.5 mm. In the sensor hole a drilled through screw is used to compress a gasket around the sensor needle in order to ensure a proper seal. The top lid is sealed with an O-ring. Compression of the material can be controlled by inserting non-compressible spacers between the body and one of the lids of the device.

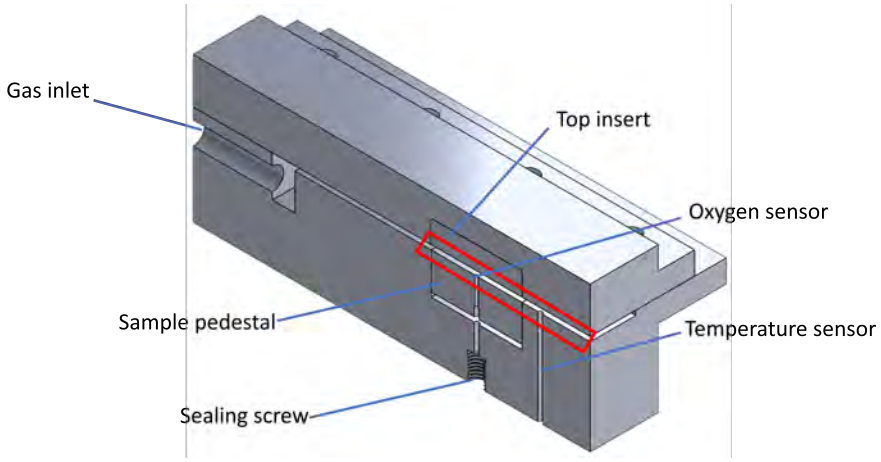

Figure 9: Final design of the through-plane device. The red box denotes the area of the flow simulation in Figure 10b

4.2 Through-plane

The design for the through-plane measurements consists of several parts. A main body with a connection for the gas inlet which then flows into a rectangular channel which raises up into a 1 mm high and 20 mm wide channel. This channel is open at the top and is closed by a lid. Towards the end of this channel a deeper cavity is made which can hold the sample pedestal which is adjustable in height in order to control compression. Again a drilled through screw is used to compress a gasket to ensure no oxygen leaking. Downstream from the sample area is a hole for the temperature sensor. The lid for this device is a flat plate with flanges for closing the device. At the location of the sample pedestal an indent is made in the lid which can fit an insert which holds the sample in place. Furthermore, this insert can be replaced with shaped insert to mimic flow field geometry. Due to the adjustability of the sample pedestal it is possible to test both single GDLs and stacks of GDLs.

4.3 Flow Simulations

Solidworks has a built in functionality that can perform computational fluid dynamics simulations on the 3D models made with the software. Before the manufacture of the devices a flow simulation was done to get an insight to how well the boundary condition could be applied. Parallel streamlines and a flat flow profile are good indicators for proper

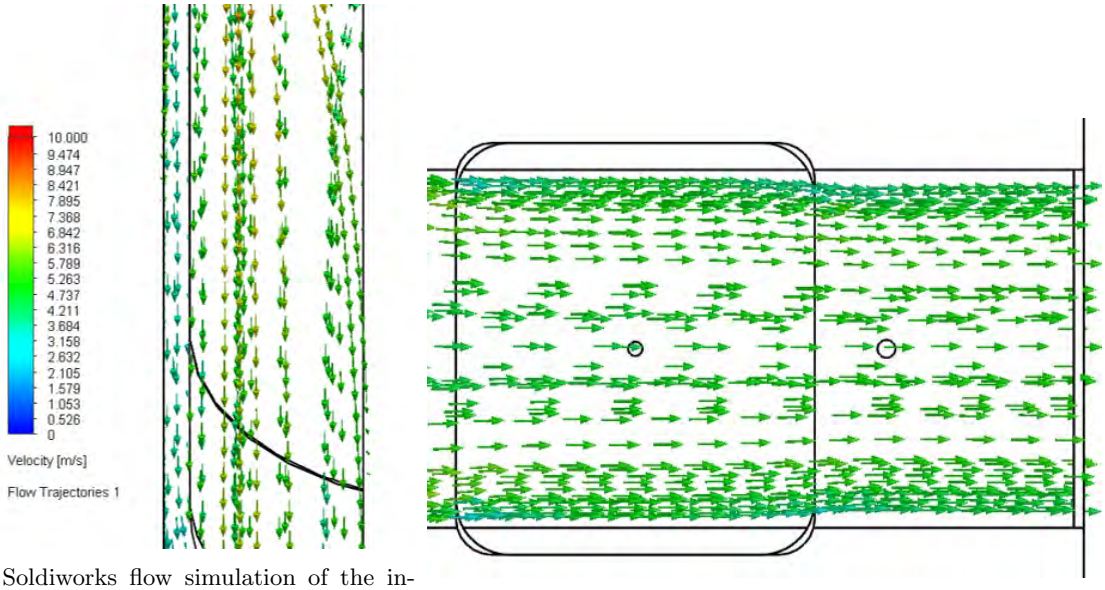

(a) Soldiworks flow simulation of the in-plane device

(b) Solidworks flow simulation of the through-plane device

Figure 10: Solidworks flow simulations done at a flow rate of 6 $\frac{l}{min}$

application of the boundary conditions.

The simulation results for the in-plane device can be seen in Figure 10a. The shown section is represented in the red box of Figure 8b. The streamlines are parallel at the sample stage but not entirely flat. This is likely due to the four inlet holes at the top of the device compared to the eight outlets. The outlets lining up with the inlets provide a path of least resistance and thus a higher flow rate. However across the board this flow is still fast enough to properly apply the boundary condition to the material. Figure 10b shows the flow simulation in the through plane setup in the red box of Figure 9. Even though the streamlines converge towards the outlet of the device, the flow around the sensor should still be uniform enough for the measurements

5 Experimental

The experimental setup consists of the in-plane device described in the previous section, a Pyroscience Firesting O_2 oxygen/temperature meter connected to a computer running Pyroscience workbench, a Pyroscience PT100 temperature sensor, a Pyroscience 430 OXR-UHS oxygen sensor, a King 7510 series model 2B-03 and, an MBP series 630 flow meter.

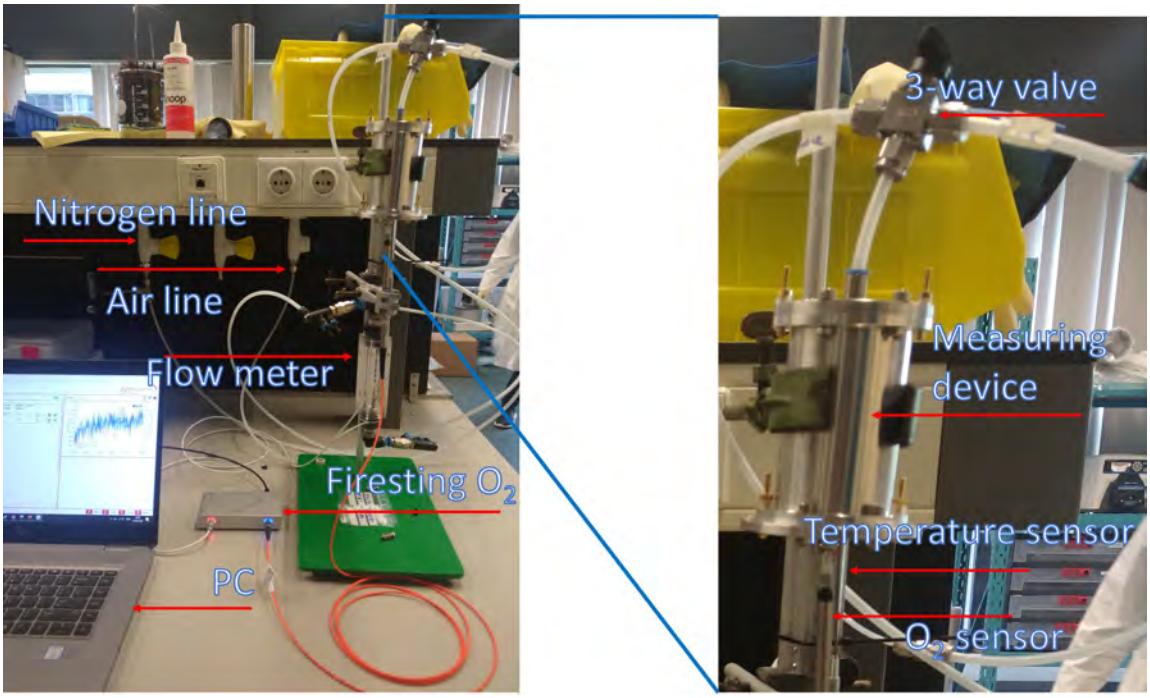

Figure 11: Photo of the experimental setup

The device is connected to the air and nitrogen lines with a three way valve. The nitrogen line also passes through the flow meter. An annotated photo of the experimental setup can be seen in Figure 11 and a schematic of the setup in Figure 12.

Two experiments were performed in this setup, open gap experiments to verify the working of the device and diffusion measurements on GDL materials. First for all experiments the sensor was calibrated using Pyroscience workbench in both air and nitrogen. Before starting a measurement a steady air flow was flowed through the device until the oxygen concentration readout did not change anymore. Also the desired flow rate for the nitrogen stream was set. After starting the data recording this airflow was maintained for 10 seconds after which the flow was switched to the nitrogen stream. This flow was maintained until the oxygen concentration did not change anymore at which point the data recording was stopped. Between measurements the parameters of interest could be changed such as the gas flow rate and open gap size for the open gap experiments and the degree of compression for the GDL experiments.

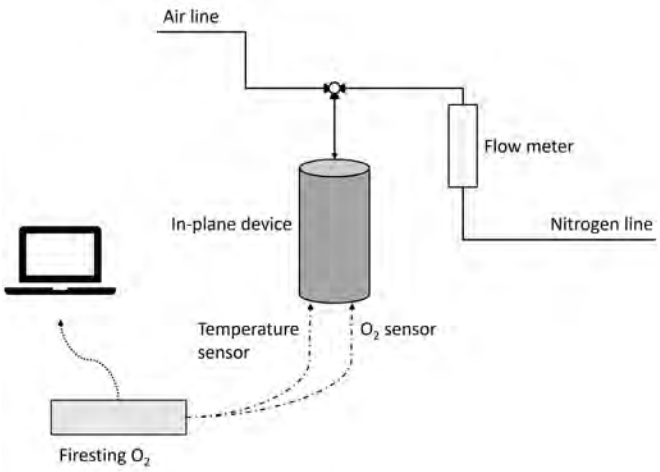

Figure 12: Schematic of the experimental setup

For the open gap experiments the flow rate was varied within the boundaries of the two flow meters which is $1 - 5\ \frac{l}{min}$ for the MBP 630 series and $28.3 - 73.6\ \frac{l}{min}$ for the King 7510 2B-03 meter. The gap was varied between $50 - 900\ \mu m$. The GDL experiments were performed at a flow rate of $28.3\ \frac{l}{min}$ with Freudenberg H15 untreated carbon paper, Freudenberg H15C14 PTFE treated GDL with an MPL, Elat hydrophyllic cloth, Avcarb G100 carbon felt, and a material made using Non-solvent Induced Phase Separation (NIPS) in house. For the Freudenberg H15C14 paper the MPL was positioned on the top so it would not impede the mass transfer and could be compared to the untreated Freudenberg H15. The NIPS material was positioned with the smaller pores on the sensor side in order to compare the positioning with the greatest mass transfer resistance to the commercial materials. The range of compression for the commercial materials is 10%-40% while the range of compression for the NIPS material is 1.5%-10%.

6 Diffusion Modeling

The data from the Pyroscience sensor is obtained as oxygen concentration over time. In order to extract an effective diffusion coefficient from this data a computational model was written to fit Fick's second law to the data that was obtained experimentally by actuating the diffusion coefficient.

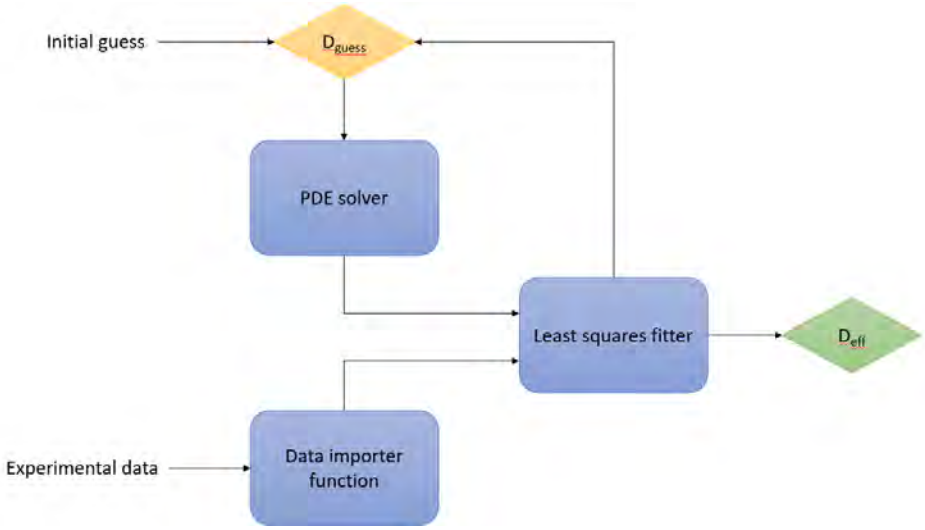

Figure 13: Schematic representation of the MATLAB model

6.1 MATLAB model

The overall schematic of the MATLAB model is given in Figure 13. Two inputs are given, the dataset obtained experimentally and an initial guess for the effective diffusion coefficient. This initial guess is used to generate a concentration over time solution with a numerical PDE solver. This solution is then subtracted from the experimental data set to obtain the set of errors between the model and the dataset. This error set in then input into the least squares fitter which adjusts the diffusion coefficient, this new diffusion coefficient is then used to solve Fick's second law again and generate a new error set. The least squares fitter continues this process until the sum of the squares of the error set is minimized.

The general PDE that is solved in this model is Fick's second law in 1-D

$$\frac{\partial c}{\partial t} = \frac{D_{eff}}{r^m}\frac{\partial}{\partial r}(r^m \frac{\partial c}{\partial r}) \tag{17}$$

Where m is a geometry factor which is 0 for slab geometry, 1 for cylindrical geometry and 2 for spherical geometry. For all simulations involving the in-plane device cylindrical geometry will be used.

The MATLAB model is primarily based on two functions provided by MATLAB, `pdepe`

and `lsqnonlin` and one custom function for importing data. `pdepe` is a PDE-solver that can solve 1-D parabolic and elliptic PDEs by applying the Method Of Lines, in this case the PDE is discretized along the spatial domain into a system of ODEs. This system of ODEs is then solved by the inline MATLAB function `ode15s` which uses a backward step variant of the Numerical Differentiation Formulas (NDFs) of order 1-5. The general equation for the NDFs is given as[26]

$$\sum_{m=1}^{k} \frac{1}{m} \nabla^m y_{n+1} - hF(t_{n+1}, y_{n+1}) - \kappa\gamma_k(y_{n+1} - y_{n+1}^{(0)}) = 0 \tag{18}$$

With

$$y' = F(t_{n+1}, y_{n+1}) \tag{19}$$

Where k is the order of the formula, y_{n+1} is the value of the function at the next time step, h is the size of the time step. κ is a constant used to balance error size and stability, $\gamma_k = \sum_{j=1}^{k} \frac{1}{j}$ is a weighing factor based on the order of the NDF, and $y_{n+1}^{(0)}$ is a predicted value of y_{n+1} as

$$y_{n+1}^{(0)} = \sum_{m=1}^{k} \nabla^m y_n \tag{20}$$

`ode15s` uses a variable order algorithm to integrate the system of ODEs created by `pdepe`. Since a backward step method is used to integrate these equations time step size is not a stability concern and the same time step can be used as those from the experimental data.

The MATLAB function `lsqnonlin` is a function that minimizes the squares of an objective function which in this case is the error set between the solution provided by `pdepe` and the experimental data set. This minimization is done by varying D_{guess} as can be seen in Figure 13. The method used by `lsqnonlin` is the trust region reflective algorithm which uses a 2^{nd} order Taylor expansion of the function around the variable D_{guess} within the maximum allowed step size. It then searches for the most optimal value of D_{guess} within this trust region. This is repeated until a minimum of the objective function is found. The main reason for using `lsqnonlin` is that it has the functionality to execute any custom

function within its routine which allows it to use `pdepe` for iterating on D_{guess}.

Finally a mismatch between the experimental data and the solution of Fick's second law needs to be rectified. Since the experiments have a time of baseline measurement before the gas streams get switched the exact moment the initial condition gets applied to the system is unknown. In order to remedy this the data will be cut at a point during import. The initial guess for this cut is made at the point after which the data shows eight sequential decreasing points. This is sufficient to rule out pure noise from the measurements, however it is still not possible to tell whether this point is the appropriate point to cut off the dataset as random noise before the initial condition is applied might still include two or three sequential decreasing points. So the whole fitting process is done for several cutoffs around this initial guess of the cutoff point. After which the cutoff that produces the fit with the lowest sum of squared errors is used as the proper cutoff to match the initial condition of the computer model with that of the experimental setup.

6.2 Model validation and verification

In order to check whether this computer model functions adequately it is validated by checking the behaviour of the model at limiting cases and theoretically known cases. The three cases that will be used are

1. Transient simulation in slab geometry with $D_{eff} = 0$
2. Transient simulation in slab geometry where the initial condition and the sample edge boundary condition have the same value
3. Steady state simulation in slab geometry with two constant boundary conditions

Case one represents a system where no transport could take place because the transport paths are completely blocked. Case two represents a system where the flow valve is never switched over to another gas flow. Case three represents a system where on one side of the sample air is continuously flowed past the while on the other side of the sample nitrogen is flowed past. As seen from the graphs in Figure 14 all three case show the expected behaviour.

In order to verify that `lsqnonlin` works as expected a data set is generated by solving the

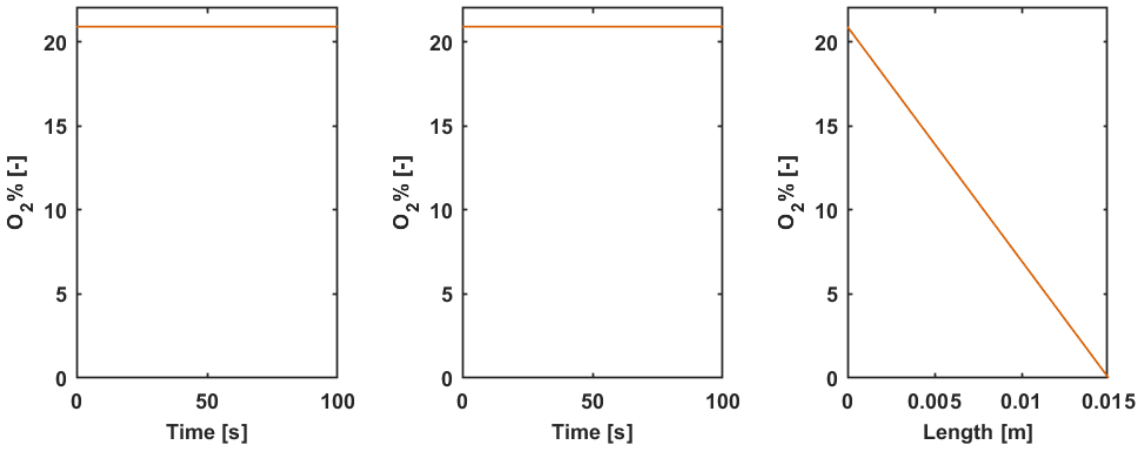

(a) Case 1 (b) Case 2 (c) Case 3

Figure 14: Validation cases

PDE in cylindrical coordinates with a diffusion coefficient $D = 1 \cdot 10^{-5}\ \frac{m^2}{s}$ and a domain size of 15 mm. Then this solution was input into the fitting model with an initial guess for the diffusion coefficient of $D_{guess} = 5 \cdot 10^{-5}\ \frac{m^2}{s}$. The resulting fit is seen in Figure 15. The fitted diffusion coefficient is the same as the one used to generate the data set.

After validating the model with these boundary cases it is also important to verify the model using data sets of transient diffusion processes found in literature. The two cases used for verification are

1. A bulk diffusion experiment by Astrath et al. using a Loschmidt cell [27]
2. A bulk oxygen diffusion experiment by Kim & Gostick using a device very similar to the one presented in this thesis [21]

For both these cases the data was extracted from the graphs presented in the papers. For the experiment by Astrath et al. the data did not line up nicely with the diffusion model. For the experiment by Kim and Gostick the model and data coincided nicely.

The first case is based on an experiment performed by Astrath et al. using a Loschmidt cell for determining oxygen diffusion in humidified conditions. Their control experiment in dry conditions is used in order to verify the MATLAB model. The apparatus they used is a vertical cylinder of 35.5 cm and has two chambers separated by a ball valve where

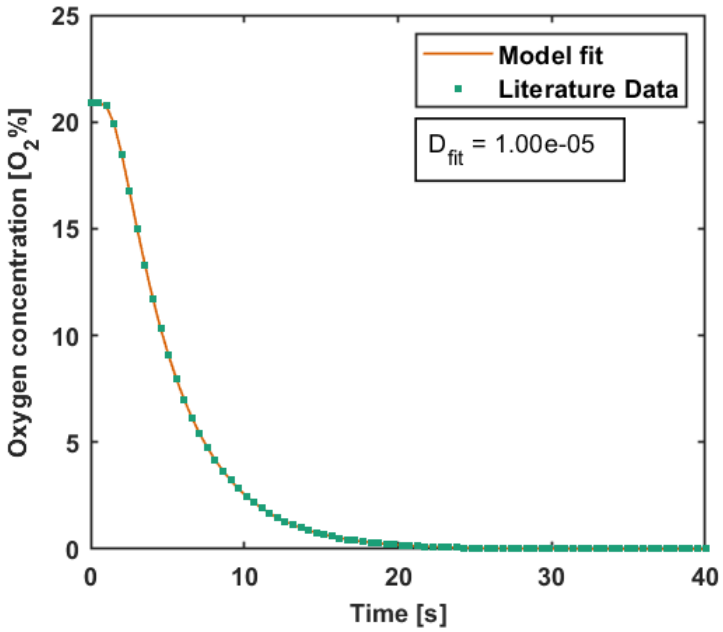

Figure 15: Fit with `lsqnonlin` of a data set generated by solving the diffusion equation numerically

the lower chamber is filled with pure O_2 and the upper chamber is filled with pure N_2. An optical fiber probe oxygen sensor is placed in the upper chamber 1.9 cm from the valve. The experiment is conducted by opening the ball valve and letting the gases diffuse into one another. The following initial and boundary conditions are used to simulate this experiment using Fick's second law in a slab geometry

$$\begin{aligned} t = 0 \quad & \begin{cases} -L < z < 0, \quad C = 100\% \\ 0 < z < L, \quad C = 0\% \end{cases} \\ t > 0, \quad & z = \pm L, \quad \frac{\partial C}{\partial z} = 0 \end{aligned} \tag{21}$$

Where L is the length of a compartment which is 17.75 cm.

The data obtained from the graph does not provide enough resolution to accurately assess the actual start of the diffusion process. Therefore, an interpolation of the data was made

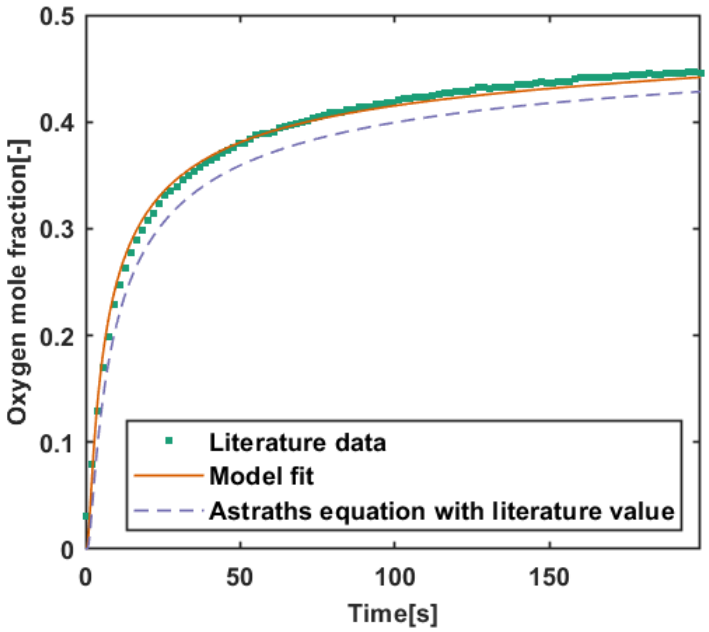

Figure 16: Validation using the data by Astrath et al. [27]

to give a finer idea of the start of the process. The data was cut off at different proposed times for t_0 and for each of these cases the model was used to fit a diffusion coefficient to this data. Unfortunately, even for the cutoff with the smallest error the solution obtained by fitting the least squares does not align nicely with the data points from the publication by Astrath et al as the residuals are unbalanced. Furthermore, the value of t_0 giving the best fit corresponds to a concentration data point larger than 0. Which should not be possible. In order to double check this result the penetration theory solution provided by Astrath et al. were compared with the experimental data using the value of D_{eff} given by Astrath et al. This solution also does not align with the data points. The most likely cause of this discrepancy is the graph in the paper by Astrath et al. not being accurate enough to properly extract these data points from. Finally the diffusion coefficients found by Astrath et al, the value fitted with the model and, the predicted value by Chapman-Enskog theory are presented in Table 1.

The second verification case is based on an experiment performed by Kim & Gostick uses a device similar to the one described in this thesis. Featuring two cylindrical pedestals

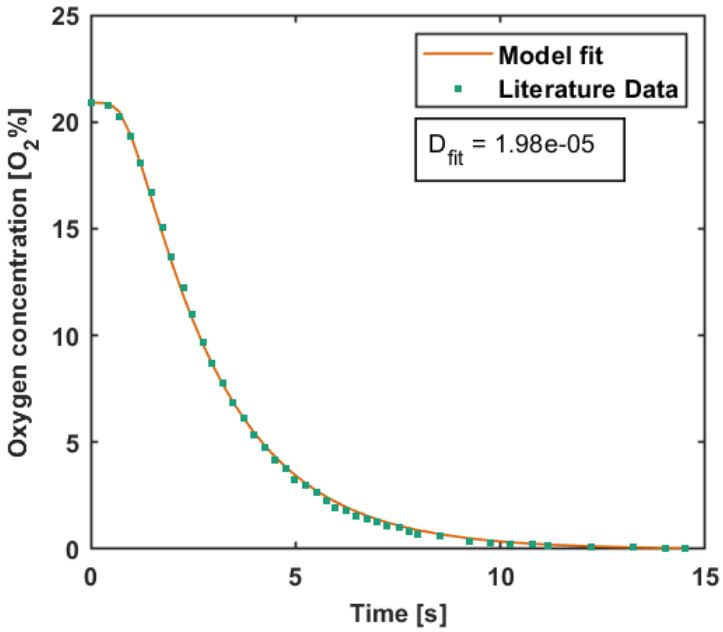

Figure 17: Model fit to the data of Kim & Gostick

with a space in between for the sample and the oxygen sensor in the center of the disk. For verification purposes these experiments were carried out using an open gap by flowing pure nitrogen past the sides of the pedestals. The resulting diffusion coefficient from this experiment corresponds with the literature value of $2.02 \cdot 10^{-5}\ \frac{m^2}{s}$. In order to check the model these experimental data points were copied and imported into the model where Fick's second law with the following initial and boundary conditions

$$\begin{aligned} t = 0, \quad & 0 < r < R \quad C = 20.9\% \\ t > 0, \quad & r = R \quad C = 0\% \\ t > 0, \quad & r = 0 \quad \frac{\partial C}{\partial r} = 0 \end{aligned} \tag{22}$$

The resulting fit can be seen in figure Figure 17. The diffusion coefficient obtained by the MATLAB model is $1.98 \cdot 10^{-5}\ \frac{m^2}{s}$ which falls in the error margin of $\pm 6.06 \cdot 10^{-7}\ \frac{m^2}{s}$ reported by Kim & Gostick. A likely source for this inaccuracy is the reported number was

	Literature value $\frac{m^2}{s}$	Model value $\frac{m^2}{s}$	Chapman-Enskog value $\frac{m^2}{s}$
Least squares test	$1 \cdot 10^{-5}$	$1 \cdot 10^{-5}$	N/A
Astrath et al.	$2.78 \pm 0.03 \cdot 10^{-5}$	$3.93 \cdot 10^{-5}$	$2.72 \pm 0.16 \cdot 10^{-5}$
Kim & Gostick	$2.02 \pm 0.067 \cdot 10^{-5}$	$1.98 \cdot 10^{-5}$	$2.06 \pm 0.12 \cdot 10^{-5}$*

Table 1: Literature data compared with the fits made by the MATLAB model. *No temperature and pressure data were available for the experiments by Kim & Gostick so these were estimated

generated from multiple experiments while this fit is only done on the data points from one experiment.

7 Results

The experiments that were performed serve two main purposes. Firstly, open gap experiments were performed to verify the working of the device. Secondly, GDL materials were measured to determine their in-plane diffusivity.

7.1 Open gap experiments

Figure 18 shows a typical data set obtained from an open gap experiment and the fit of Fick's second law to the data. The experimental procedure records a baseline so a proper value for the initial condition can be extracted. Due to this the start of data recording does not line up exactly with the moment where the outer boundary condition is applied. The procedure for determining this point is described in the section 6.1 on the MATLAB model.

As can be seen in Figure 18 the model does not properly align with the data gathered. The fit overestimates the oxygen concentration close to t_0 and it underestimates the concentration at later times. As such it does not follow the shape of a pure diffusion curve. At low oxygen concentration the model shows a higher speed of the mass transport. The expected result of the open gap experiments is to find a value for the diffusion coefficient of $2.2 \cdot 10^{-5}$ $\frac{m^2}{s}$ for oxygen-nitrogen diffusion which corresponds to the literature[21]. Instead, the found diffusion coefficient is smaller than the expected literature value. The largest issue with this method of fitting is that the choice of cutoff point on the low oxygen right side of the data set influences the value that is found for the diffusion coefficient. Judging

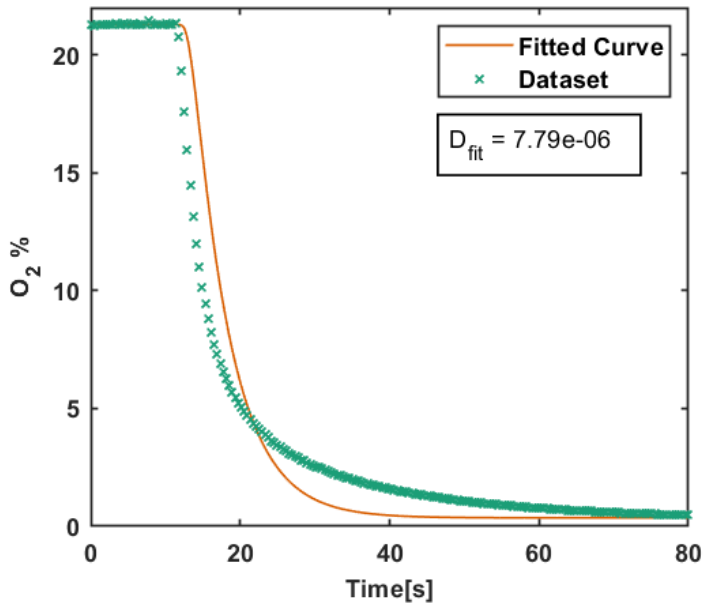

Figure 18: Typical concentration profile fitted with the model with a gap of 50 μm and with a superficial gas velocity of 1.8 $\frac{m}{s}$

from the results the data does not represent pure diffusion and as such an extended tail end of the graph changes the fit of Fick's law with the smallest error that can be made. This lead to the decision to only fit Fick's second law to the part of the data with an oxygen concentration above 14% as shown in Figure 19 with the same data set as Figure 18. This method gives a consistent standard in order to compare all the measurements taken. The diffusion coefficient found with this method, although closer, is still not close to the literature value.

7.2 Superficial Velocity

The next parameter to determine is the superficial gas velocity at which these experiments need to be carried out. Figure 20 shows a qualitative expected relation between the diffusion coefficient and the superficial gas velocity. At low gas velocities the initial condition for instantly switching the boundary value to 0% oxygen does not get imposed properly. At high gas velocities it is likely that convection will occur within the sample region of the apparatus increasing mass transfer and leading to inflated diffusion coefficients from fitting

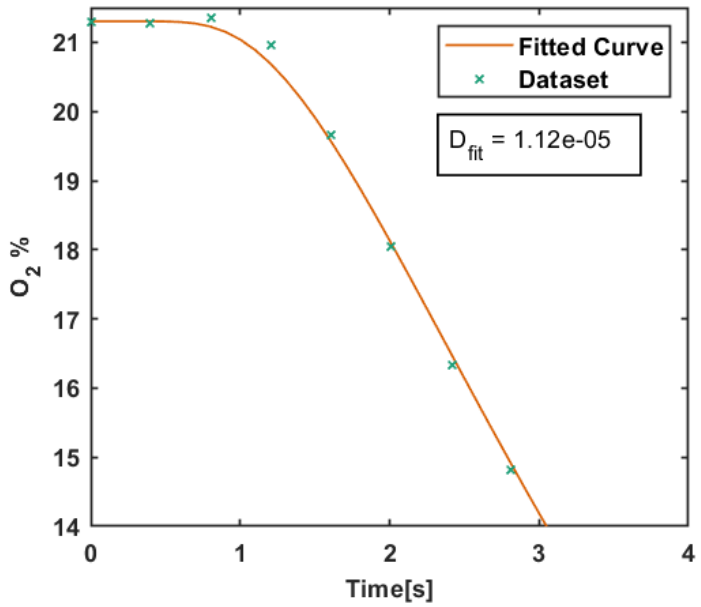

Figure 19: Typical fit up to 14% O_2 concentration with a gap of 50 μm and with a superficial gas velocity of 1.8 $\frac{m}{s}$

Fick's 2nd law. The middle flat region is the desired region where no convection into the sample area occurs but the initial condition does get imposed properly. In this region the height of the gap and the exact flow rate should not influence the mass transfer of oxygen out of the sample area.

The experiments were carried out between a superficial gas velocity of 0.065 and 0.33 $\frac{m}{s}$ and 1.8 to 4.8 $\frac{m}{s}$. Which correspond to a Reynolds number between 10.4 and 52.3 and 296 to 770 respectively. This is within the boundaries for laminar pipe flow however at these higher velocities the likelihood that entrance effects or eddies generated at the edges of the pedestal generate additional mass transfer increases. For each gas flow rate six experiments were carried out at different times. The results of these experiments is shown in Figure 21, and the error bars show one standard deviation from the average. Generally the trend in both of these regions is a positive correlation between superficial gas velocity and diffusion coefficient. And although the higher flow rates do yield results close to the literature value of diffusion, these results could not be consistently reproduced. This is in contrast to the findings of Kim & Gostick as shown in Figure 23. Combining the findings of the low and

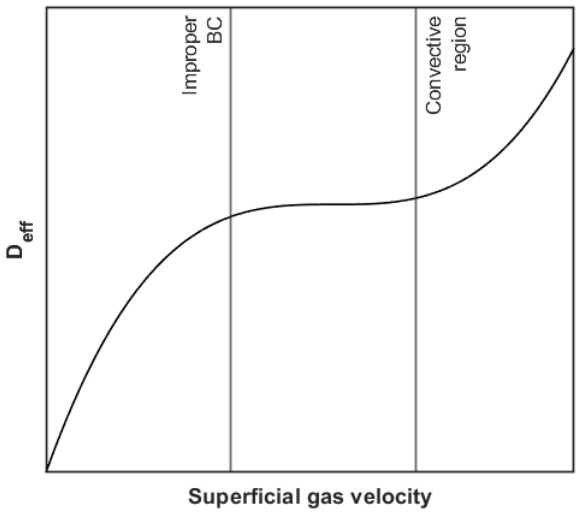

Figure 20: Expected relation between superficial gas velocity and diffusion coefficient

high flow rate experiments, the region between these two sets of experiments seems to be the flattest region which would make it the most desirable to do experiments in.

Since the range of flow rates that can be operated in is determined by the different flow meters available the superficial gas velocity was increased by reducing the sample pedestal-wall gap by inserting a 3D printed hollow cylinder with a thickness of 0.75 mm. The results of these experiments can be seen in Figure 21. Interestingly the diffusion coefficients found with this increased superficial gas velocity is not markedly different from the coefficients found with the same flow rate but a lower superficial gas velocity.

7.3 Gap height

Using spacer materials the gap height of the open gap was varied between 0.05 and 0.9 mm at a superficial gas velocity of 0.20 $\frac{m}{s}$. For each gap size three experiments were carried out. The results of these experiments can be seen in Figure 22. This figure shows a positive correlation between the gap height and the diffusion coefficient. In the case of pure diffusive behavior the height of the open gap should not influence the mass transfer rate. However, the positive correlation between gap height and hints at possible non-diffusive behaviour occurring withing the device. A comparison between the results obtained in our

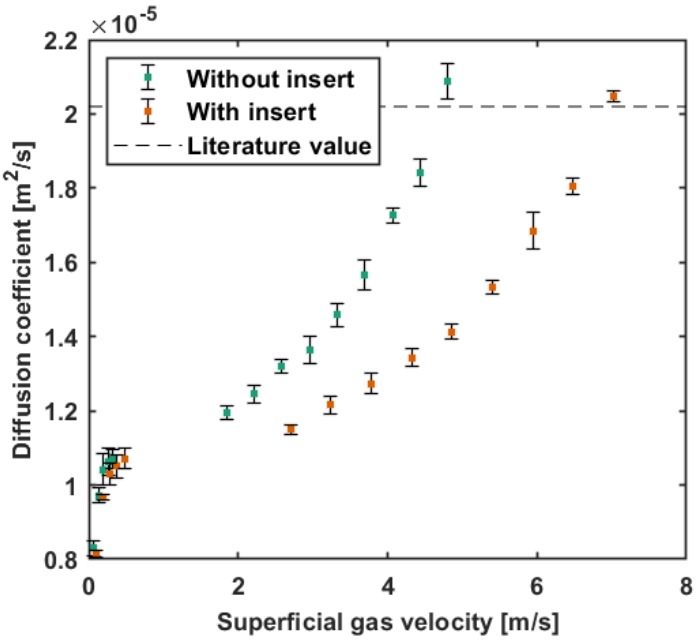

Figure 21: Diffusion coefficients at different superficial gas velocities with a reduced pedestal-wall gap with a gap height of 50 μm

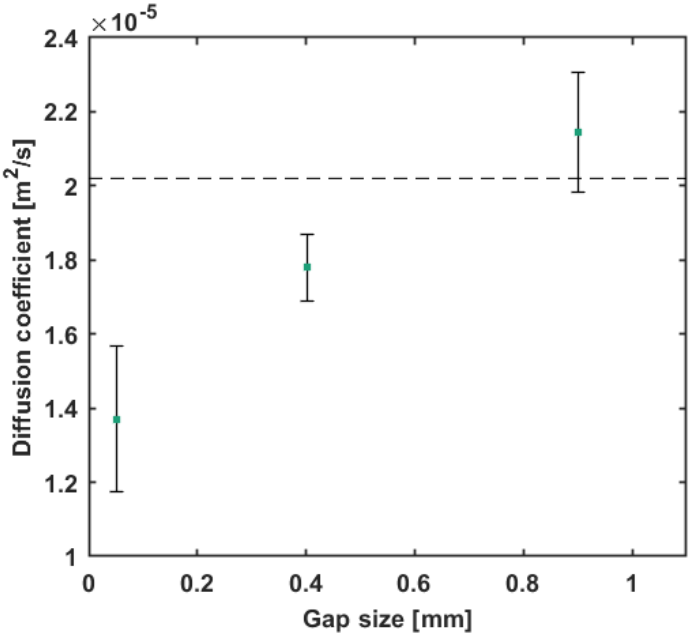

Figure 22: Diffusion coefficients at different gap sizes at a superficial gas velocity 0.20 $\frac{m}{s}$

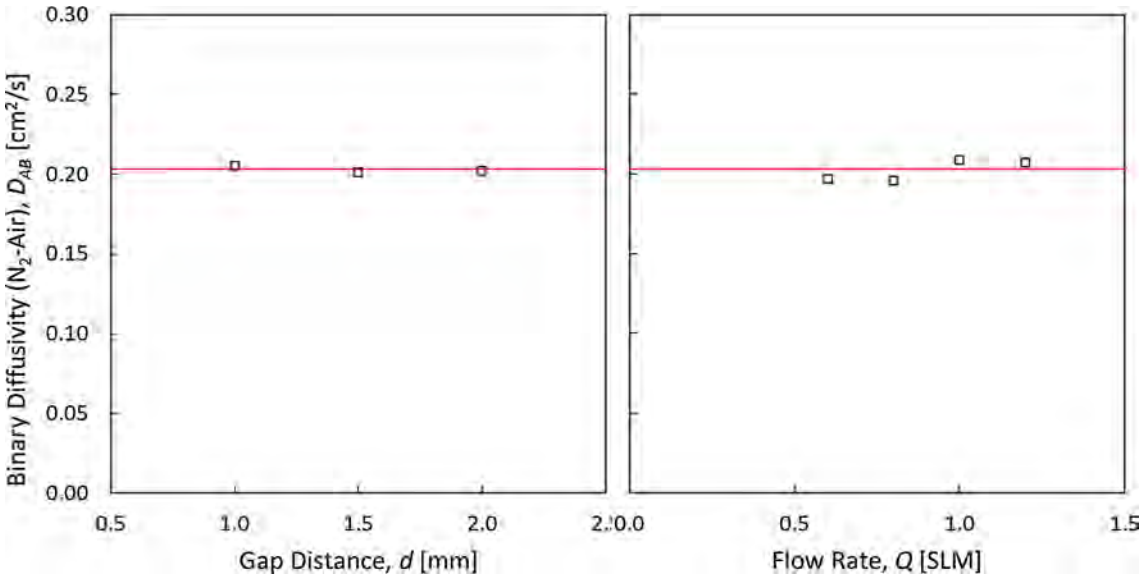

Figure 23: Open gap experiments with different gap sizes and gas flow rates performed by Kim & Gostick[21]

experiments and those obtained by Kim & Gostick as shown in Figure 23 further supports this hypothesis.

7.4 Further Troubleshooting

Several possible causes for the non-diffusive behaviour were investigated. These were leaks in the device, improper alignment of the pedestals, the influence of dead space in the device, back mixing, and leakage through the gas lines. The leakage was investigated by submerging the device in water and running nitrogen gas through it. This did not show any places where visible bubbles emerged from any seams or sealing. The improper alignment was addressed by using banana plugs which center in the screw holes because of their spring like behaviour. This more securely centered the device than just using bolts which have some leeway inside the holes. **??** shows that this did not lead to a significant difference in the data obtained. The diffusion coefficient without the plugs is $1.37 \cdot 10^{-5}$ $\frac{m^2}{s}$ and $1.32 \cdot 10^{-5}$ $\frac{m^2}{s}$ with plugs. The difference between the two profiles is within the regular variation observed in experiments.

A significant volume of dead space in the top section of the device is thought to be a cause for the slower than expected diffusion rates observed as this dead space might unintention-

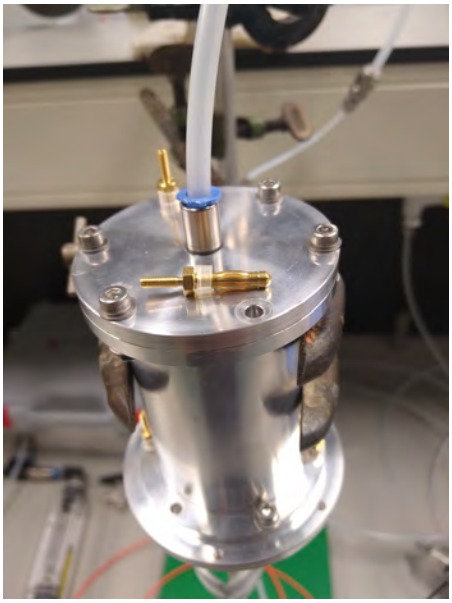

(a) Banana plugs in the device

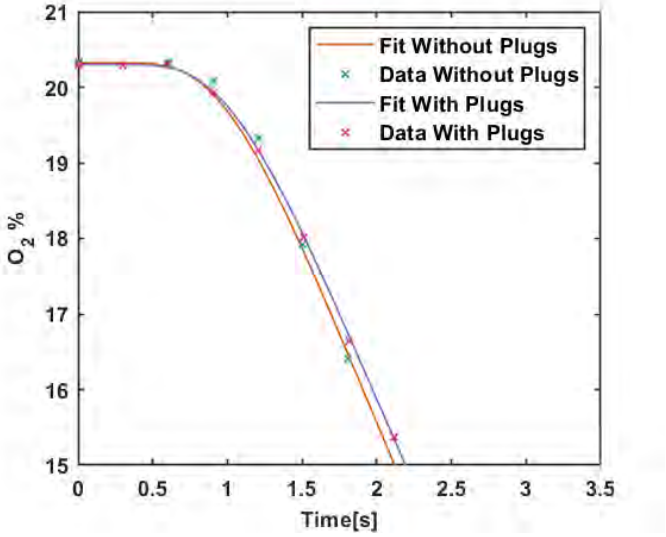

(b) Influence of the banana plugs on the concentration profile with a gap of 50 μm and a superficial gas velocity of 0.20 $\frac{m}{s}$. $D_{without} = 1.37 \cdot 10^{-5}\ \frac{m^2}{s}$ $D_{with} = 1.32 \cdot 10^{-5}\ \frac{m^2}{s}$

Figure 24: Banana plug influence on concentration profiles and implementation in the device

ally increase the oxygen content of the gas being flowed past the sample area. This dead space in the top of the device was addressed by including a 3D printed element designed to fill up this space shown in Figure 25a. The comparison between the concentration profiles obtained before and after the implementation of the space filler element are shown in Figure 25b. The diffusion coefficient without the plugs is $1.45 \cdot 10^{-5}\ \frac{m^2}{s}$ and $1.48 \cdot 10^{-5}\ \frac{m^2}{s}$ with the filler. The diffusion with the space filler element occurs slightly faster than without but is still within the natural variation seen in experiments.

Back mixing can occur in this device due to uneven pressure distributions over the outlet holes, where air possibly can flow back into the device through the holes not aligned with the inlet holes while nitrogen flows out through the holes that are aligned. Since the pressure drop over the entire device was too small to measure with the manometer on hand ($\Delta p < 0.01\ bar$) it is hard to say whether this is likely to occur. However it was still thought prudent to investigate. The possibility of back mixing was investigated by limiting the outlet holes in the bottom of the device by taping them shut and subsequently puncturing them with a needle. This was done to increase the pressure in the device and

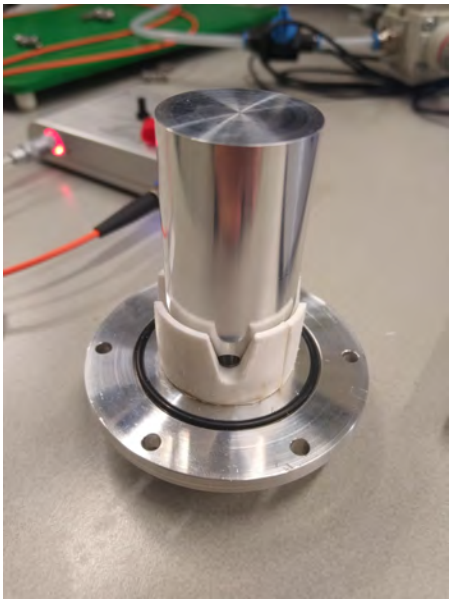

(a) Dead space filler in the device

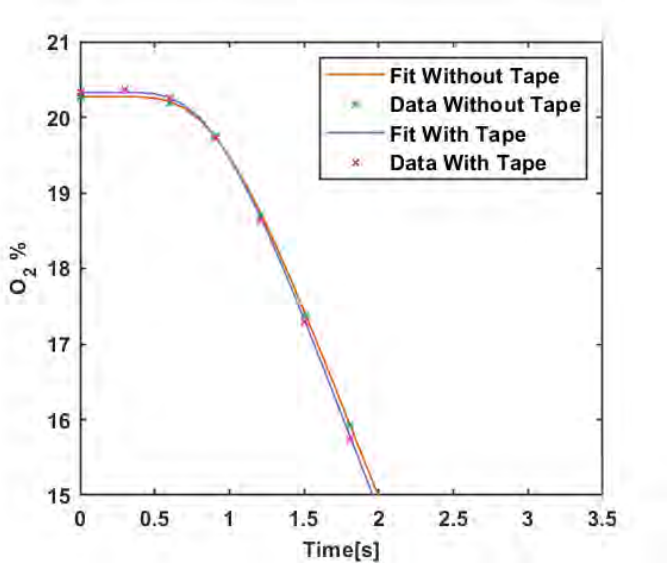

(b) Influence of the dead space filler on the concentration profile with a gap of 50 μm and a superficial gas velocity of 0.20 $\frac{m}{s}$. $D_{without} = 1.45 \cdot 10^{-5}\ \frac{m^2}{s}$ $D_{with} = 1.48 \cdot 10^{-5}\ \frac{m^2}{s}$

Figure 25: Dead space filler influence on concentration profiles and implementation in the device

as such to limit the possibility of flow back into the device. The resulting concentration-time curves as seen in Figure 26 are significantly different from one another. The diffusion coefficient without the tape is $1.45 \cdot 10^{-5}\ \frac{m^2}{s}$ and $5.52 \cdot 10^{-5}\ \frac{m^2}{s}$ with the tape. This is thought to be due to an unintended side effect of the increase in pressure inside of the device which has a significant influence on the oxygen concentration recorded by the Pyroscience sensor. However without a pressure sensor inside of the device this is impossible to confirm.

Besides non-diffusive behaviour another issue that impacts these measurements is the non-linearity of the relation between the directly measured quantity, the phase shift, and the oxygen concentration. Which prevents a simple two point calibration. Since the calibration method used by the Pyroscience device is reliant on control of the temperature, the pressure and the humidity of the gases which is not possible in the current setup. A custom 3- or 4-point calibration is desirable. Unfortunately this was not feasible in the scope of this research.

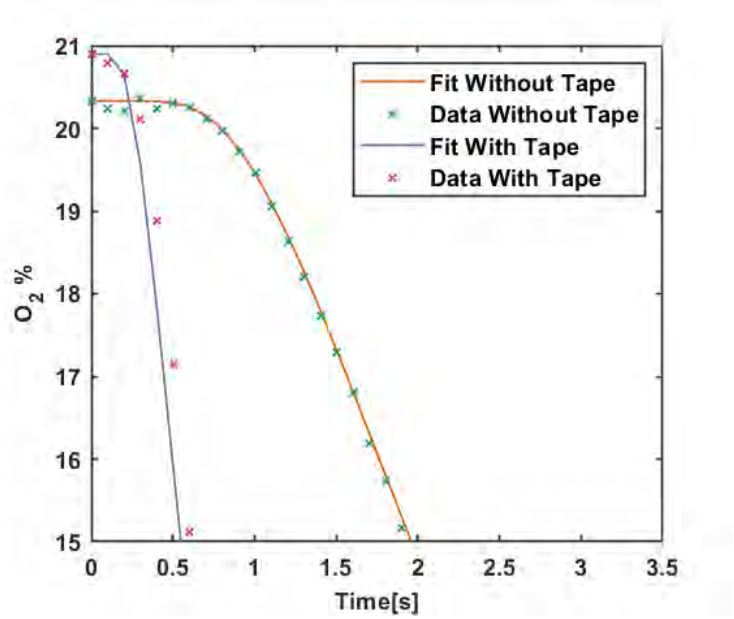

Figure 26: The influence of taping the gas outlets with a gap of 50 μm and a superficial gas velocity of 0.20 $\frac{m}{s}$. $D_{without} = 1.45 \cdot 10^{-5}$ $\frac{m^2}{s}$ $D_{with} = 5.52 \cdot 10^{-5}$ $\frac{m^2}{s}$

7.5 GDL materials

Even though the exact numerical results of the open gap experiments do not correspond to the literature value of the oxygen-nitrogen diffusion coefficient, the results from this device can still be used to qualitatively compare different GDL materials. Five materials were selected for this analysis. Freudenberg H15 carbon paper, Freudenberg H15C14 carbon paper with an MPL and hydrophobic treatment, Elat hydrophillic cloth, Avcarb G100 carbon felt and a material made using Non-solvent Induced Phase Separation (NIPS) in the research group. The Freudenberg (FB) papers were selected because carbon papers are the most widely researched GDL materials, furthermore it is of interest to research the impact of the hydrophobic treatment on the diffusion characteristics of these materials. The cloth and felt were selected as these are materials that are considered for GDLs that have base structure that is different from the carbon papers that are available on the market. Finally the material based on NIPS was investigated as this is a novel material that is investigated as a GDL and it is of interest to see how it compares to available commercial materials. Of the commercially available materials three samples were studied at four degrees of compression.

	Thickness $[\mu m]$	Areal Weight $[\frac{g}{m^2}]$	Porosity* $[-]$	Compression Range $[\%]$	D_{eff} range $[\frac{m^2}{s}]$
FB H15	144	66.1	0.80	10.1-41.7	1.10-1.23
FB H15C14	177	90.8	0.77	6.4-40.2	0.753-0.872
Elat Cloth	308	115	0.83	8.3-39.5	1.26-1.57
Avcarb G100	3430	300	0.96	9.8-40.1	2.03-2.25
NIPS PS-65-3	510	101	0.91	1.5-9.7	1.58-1.60

Table 2: Data of the investigated GDL materials *The porosity was estimated using the density of the material and the density of carbon

Figure 27 shows the results of a compression study done on the four commercially available GDL materials. In general it show a slightly decreasing trend in diffusion coefficient with increasing compression. The larger error bars on the compression for the FB materials is due to their thinness combined with only certain thicknesses of spacer materials being available leading to less relative control on the degree of compression. Another strong caveat to place with these results is that the Avcarb G100 felt has a thickness of about 3.4 mm while the other materials range from 0.14 mm to 0.31 mm. Since the open gap experiments showed a positive correlation between gap size and diffusion coefficient in this system it is reasonable to assume that this also affects the results for the GDL experiments. Additionally, the hydrophobic treatment of FB H15C14 possibly contributed to the decrease in diffusion in this material compared to plain FB H15.

Figure 28 shows the comparison between the commercial GDLs at low compression and the NIPS material made in house. Contrary to the commercial GDL materials the diffusion of the NIPS material does not decrease significantly with compression. Although, higher degrees of compression were not tested with this material as it is likely that the material would be destroyed by the higher pressure. In diffusion the NIPS material performs similarly to the Elat cloth and better than the Freudenberg papers.

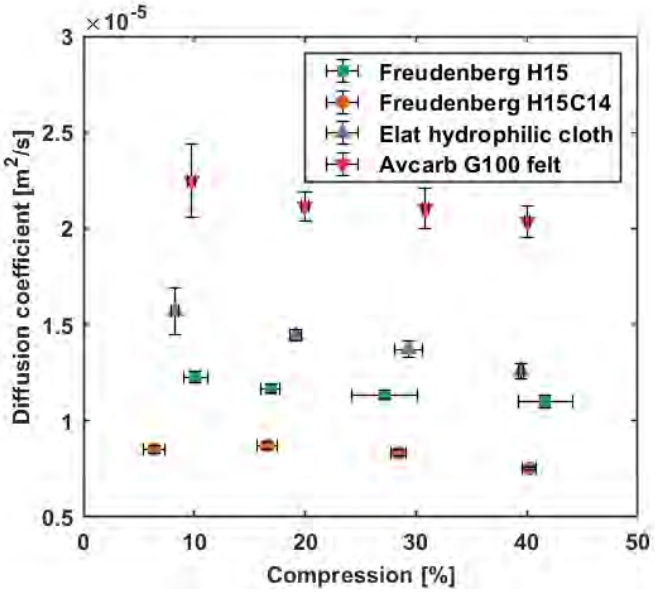

Figure 27: Effective diffusion coefficients of commercially available GDL materials at different degrees of compression at a superficial gas velocity of 1.8 $\frac{m}{s}$

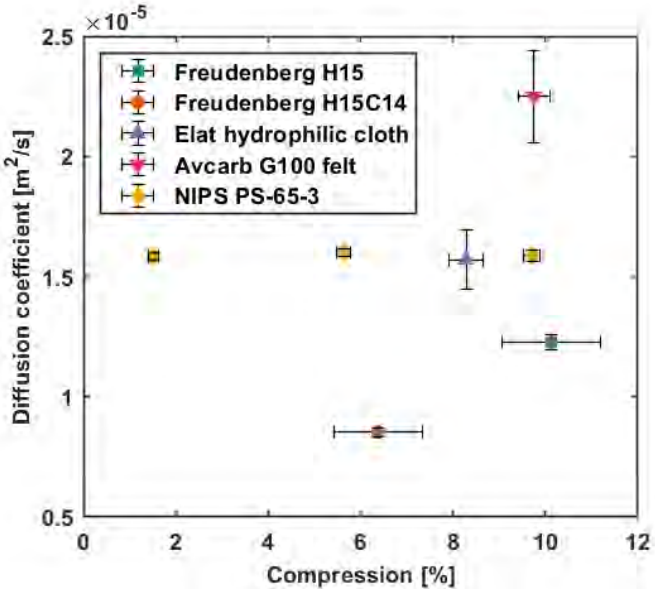

Figure 28: Effective diffusion coefficients of the NIPS material compared with commercially available GDLs at a superficial gas velocity 1.8 $\frac{l}{min}$

8 Conclusion and Outlook

Two devices for determining in- and through-plane diffusion coefficients in GDLs were fabricated. The method of measurement selected for these devices is direct transient oxygen measurement. For the processing of the data a MATLAB model was developed, validated and verified and a robust standard was developed to be able to analyze all data sets in the same way. Open gap measurements were performed in the in-plane device in order to validate the proper working of the device. Several commercial GDL materials were investigated alongside a novel material made using NIPS.

Unfortunately no proper diffusion could be measured in open gap measurements and several possible causes for this were investigated. Because of the inability to measure diffusivity properly several GDL materials were measured only qualitatively. The resulting trend of decreasing diffusion coefficients with increasing compression was the expected trend. Additionally the hydrophobic treatment of a GDL was also observed to reduce the diffusion coefficient. A novel material made by NIPS was also tested and performed similarly to commercially available materials.

For future research with the transient oxygen measurement method it is recommended to update the design of the device so pressure and humidity can be measured inside of the device. Another adaptation would be to limit the open volume in the device as much as possible to ensure laminar flow and eliminate potential pockets of oxygen. Performing a custom three or four point calibration with gas standards that have low oxygen concentrations would give a stronger insight on whether the reason for the deviation from the diffusive shape of the data sets is a physical issue or a sensing issue. However, a stronger recommendation would be to employ a different method altogether for determining diffusion in GDLs. EIS seems to be the strongest candidate when taking availability of equipment, length of experiments, and costs into account. The main drawback of this method is its sensitivity to small changes in the setup and outside influences.

References

[1] A. T. De Almeida, F. J. T. E. Ferreira, and J. A. C. Fong, "Standards for Efficiency of Electric Motors," en, *IEEE Industry Applications Magazine*, vol. 17, no. 1, pp. 12–19, Jan. 2011, ISSN: 1077-2618. DOI: 10.1109/MIAS.2010.939427.

[2] J. A. Caton, "The thermodynamic characteristics of high efficiency, internal-combustion engines," en, *Energy Conversion and Management*, vol. 58, pp. 84–93, Jun. 2012, ISSN: 01968904. DOI: 10.1016/j.enconman.2012.01.005.

[3] B. G. Pollet, I. Staffell, and J. L. Shang, "Current status of hybrid, battery and fuel cell electric vehicles: From electrochemistry to market prospects," en, *Electrochimica Acta*, vol. 84, pp. 235–249, Dec. 2012, ISSN: 00134686. DOI: 10.1016/j.electacta.2012.03.172.

[4] J. Li, Z. Du, R. E. Ruther, *et al.*, "Toward Low-Cost, High-Energy Density, and High-Power Density Lithium-Ion Batteries," en, *JOM*, vol. 69, no. 9, pp. 1484–1496, Sep. 2017, ISSN: 1047-4838, 1543-1851. DOI: 10.1007/s11837-017-2404-9.

[5] S. Petrovic and E. Hossain, "Development of a Novel Technological Readiness Assessment Tool for Fuel Cell Technology," en, *IEEE Access*, vol. 8, pp. 132 237–132 252, 2020, ISSN: 2169-3536. DOI: 10.1109/ACCESS.2020.3009193.

[6] R. Rashapov, F. Imami, and J. T. Gostick, "A method for measuring in-plane effective diffusivity in thin porous media," en, *International Journal of Heat and Mass Transfer*, vol. 85, pp. 367–374, Jun. 2015, ISSN: 00179310. DOI: 10.1016/j.ijheatmasstransfer.2015.01.101.

[7] L. R. Jordan, A. K. Shukla, T. Behrsing, N. R. Avery, B. C. Muddle, and M. Forsyth, "Diffusion layer parameters influencing optimal fuel cell performance," en, 2000. DOI: 10.1016/S0378-7753(99)00489-9.

[8] R. B. (B. Bird 1924-, W. E. 1. Stewart, and E. N. 1. Lightfoot, *Transport phenomena*, English, Revised second edition. New York: John Wiley & Sons, Inc., 2007, Section: xii, 905 pages : illustrations ; 26 cm, ISBN: 0-470-11539-4 978-0-470-11539-8 0-471-41077-2 978-0-471-41077-5.

[9] A. Ozden, S. Shahgaldi, X. Li, and F. Hamdullahpur, "A review of gas diffusion layers for proton exchange membrane fuel cells—With a focus on characteristics, characterization techniques, materials and designs," en, *Progress in Energy and Combustion Science*, vol. 74, pp. 50–102, Sep. 2019, ISSN: 03601285. DOI: 10.1016/j.pecs.2019.05.002.

[10] D. M. Tartakovsky and M. Dentz, "Diffusion in Porous Media: Phenomena and Mechanisms," en, *Transport in Porous Media*, vol. 130, no. 1, pp. 105–127, Oct. 2019, ISSN: 0169-3913, 1573-1634. DOI: 10.1007/s11242-019-01262-6.

[11] B. Saha and G. C. Schatz, "Carbonization in Polyacrylonitrile (PAN) Based Carbon Fibers Studied by ReaxFF Molecular Dynamics Simulations," en, *The Journal of Physical Chemistry B*, vol. 116, no. 15, pp. 4684–4692, Apr. 2012, ISSN: 1520-6106, 1520-5207. DOI: 10.1021/jp300581b.

[12] E. Sadeghi, M. Bahrami, and N. Djilali, "A Compact Thermal Resistance Model for Determining Effective Thermal Conductivity in the Fibrous Gas Diffusion Layers of Fuel Cells," en, in *Heat Transfer: Volume 1*, Jacksonville, Florida, USA: ASMEDC, Jan. 2008, pp. 439–447, ISBN: 978-0-7918-4847-0. DOI: 10.1115/HT2008-56158.

[13] J. C. Bachman, "Experimental Investigation And Optimization Of Polymer Electrolyte Membrane Fuel Cell Parallel Flow Fields," en, 2012.

[14] A. D. Santamaria, J. Bachman, and J. W. Park, "Cold-start of parallel and interdigitated flow-field polymer electrolyte membrane fuel cell," en, *Electrochimica Acta*, vol. 107, pp. 327–338, Sep. 2013, ISSN: 00134686. DOI: 10.1016/j.electacta.2013.03.164.

[15] J. R. Lakowicz and A. Balter, "Theory of phase-modulation fluorescence spectroscopy for excited-state processes," en, *Biophysical Chemistry*, vol. 16, no. 2, pp. 99–115, Oct. 1982, ISSN: 03014622. DOI: 10.1016/0301-4622(82)85012-6.

[16] C. Chan, N. Zamel, X. Li, and J. Shen, "Experimental measurement of effective diffusion coefficient of gas diffusion layer/microporous layer in PEM fuel cells," en, *Electrochimica Acta*, vol. 65, pp. 13–21, Mar. 2012, ISSN: 00134686. DOI: 10.1016/j.electacta.2011.12.110.

[17] K. Soukup, P. Schneider, and O. Šolcová, "Comparison of Wicke–Kallenbach and Graham's diffusion cells for obtaining transport characteristics of porous solids," en, *Chemical Engineering Science*, vol. 63, no. 4, pp. 1003–1011, Feb. 2008, ISSN: 00092509. DOI: 10.1016/j.ces.2007.10.032.

[18] W. Yoshimune, S. Yamaguchi, and S. Kato, "Insights into Oxygen Transport Properties of Partially Saturated Gas Diffusion Layers for Polymer Electrolyte Fuel Cells," en, *Energy & Fuels*, acs.energyfuels.3c00317, Apr. 2023, ISSN: 0887-0624, 1520-5029. DOI: 10.1021/acs.energyfuels.3c00317.

[19] L. M. Pant, S. K. Mitra, and M. Secanell, "Characterization of Transport Properties in Porous Media of a PEM Fuel Cell," en, in *ASME 2012 10th International*

Conference on Fuel Cell Science, Engineering and Technology, San Diego, California, USA: American Society of Mechanical Engineers, Jul. 2012, pp. 361–366, ISBN: 978-0-7918-4482-3. DOI: 10.1115/FuelCell2012-91149.

[20] J. J. Kane, A. C. Matthews, C. J. Orme, C. I. Contescu, W. D. Swank, and W. E. Windes, "Effective gaseous diffusion coefficients of select ultra-fine, super-fine and medium grain nuclear graphite," en, *Carbon*, vol. 136, pp. 369–379, Sep. 2018, ISSN: 00086223. DOI: 10.1016/j.carbon.2018.05.003.

[21] Y. Kim and J. T. Gostick, "Measuring effective diffusivity in porous media with a gasket-free, radial arrangement," en, *International Journal of Heat and Mass Transfer*, vol. 129, pp. 1023–1030, Feb. 2019, ISSN: 00179310. DOI: 10.1016/j.ijheatmasstransfer.2018.10.054.

[22] D. Kramer, S. A. Freunberger, R. Flückiger, *et al.*, "Electrochemical diffusimetry of fuel cell gas diffusion layers," en, *Journal of Electroanalytical Chemistry*, vol. 612, no. 1, pp. 63–77, Jan. 2008, ISSN: 15726657. DOI: 10.1016/j.jelechem.2007.09.014.

[23] A. Lasia, *Electrochemical Impedance Spectroscopy and its Applications*, en. New York, NY: Springer New York, 2014, ISBN: 978-1-4614-8933-7. DOI: 10.1007/978-1-4614-8933-7.

[24] A. Straatman, N. Gallego, B. Thompson, and H. Hangan, "Thermal characterization of porous carbon foam—convection in parallel flow," en, *International Journal of Heat and Mass Transfer*, vol. 49, no. 11-12, pp. 1991–1998, Jun. 2006, ISSN: 00179310. DOI: 10.1016/j.ijheatmasstransfer.2005.11.028.

[25] Y. M. Volfkovich, V. Sosenkin, and V. Bagotsky, "Structural and wetting properties of fuel cell components," en, *Journal of Power Sources*, vol. 195, no. 17, pp. 5429–5441, Sep. 2010, ISSN: 03787753. DOI: 10.1016/j.jpowsour.2010.03.002.

[26] L. F. Shampine and M. W. Reichelt, "The MATLAB ODE Suite," en, *SIAM Journal on Scientific Computing*, vol. 18, no. 1, pp. 1–22, Jan. 1997, ISSN: 1064-8275, 1095-7197. DOI: 10.1137/S1064827594276424.

[27] N. G. C. Astrath, J. Shen, D. Song, *et al.*, "The Effect of Relative Humidity on Binary Gas Diffusion," en, *The Journal of Physical Chemistry B*, vol. 113, no. 24, pp. 8369–8374, Jun. 2009, ISSN: 1520-6106, 1520-5207. DOI: 10.1021/jp900796w.